ISSN 1674-1056
http://cpb.iphy.ac.cn
http://iopscience.iop.org/cpb
中国物理 B
Chinese Physics
中国物理 Chinese Physics B

## Laser scattering, transmittance and low thermal expansion behaviors in $Y_{2-x}(ZnLi)_xMo_3O_{12}$ by forming regular grains

Xian-Sheng Liu(刘献省), Yong-Guang Cheng(程永光), Bao-He Yuan(袁保合), Er-Jun Liang(梁二军), Wei-Feng Zhang(张伟风)

**Citation:**Chin. Phys. B . 2019, 28(9): 096501 . **doi:** 10.1088/1674-1056/28/9/096501
Journal homepage: http://cpb.iphy.ac.cn; http://iopscience.iop.org/cpb

**What follows is a list of articles you may be interested in**

---

## Conductive property of $Zr_{0.1}Fe_{0.9}V_{1.1}Mo_{0.9}O_7$ with low thermal expansion

Xiaoke He(何小可), Heng Qi(戚恒), Qi Xu(徐启), Xiansheng Liu(刘献省), Lei Xu(许磊), Baohe Yuan(袁保合)
Chin. Phys. B . 2019, 28(5): 056501 . **doi:** 10.1088/1674-1056/28/5/056501

## Properties of negative thermal expansion *β*-eucryptite ceramics prepared by spark plasma sintering

Li-Min Zhao(赵利敏), Yong-Guang Cheng(程永光), Hao-Shan Hao(郝好山), Jiao Wang(王娇), Shao-Hui Liu(刘少辉), Bao-Sen Zhang(张宝森)
Chin. Phys. B . 2018, 27(9): 096501 . **doi:** 10.1088/1674-1056/27/9/096501

## Phase transition and near-zero thermal expansion of $Zr_{0.5}Hf_{0.5}VPO_7$

Jun-Ping Wang(王俊平), Qing-Dong Chen(陈庆东), Sai-Lei Li(李赛磊), Yan-Jun Ji(纪延俊), Wen-Ying Mu(穆文英), Wei-Wei Feng(冯伟伟), Gao-Jie Zeng(曾高杰), You-Wen Liu(刘友文), Er-Jun Liang(梁二军)
Chin. Phys. B . 2018, 27(6): 066501 . **doi:** 10.1088/1674-1056/27/6/066501

## Negative thermal expansion and photoluminescence in solid solution $(HfSc)_{0.83}W_{2.25}P_{0.83}O_{12\delta}$

Yuan Liang(梁源), Yong-Guang Cheng(程永光), Xiang-Hong Ge(葛向红), Bao-He Yuan(袁保合), Juan Guo(郭娟), Qian Sun(孙强), Er-Jun Liang(梁二军)
Chin. Phys. B . 2017, 26(10): 106501 . **doi:** 10.1088/1674-1056/26/10/106501

## Speckle intensity images of target based on Monte Carlo method

Wu Ying-Li, Wu Zhen-Sen
Chin. Phys. B . 2014, 23(3): 037801 . **doi:** 10.1088/1674-1056/23/3/037801

---

# Laser scattering, transmittance and low thermal expansion behaviors in $Y_{2-x}(ZnLi)_xMo_3O_{12}$ by forming regular grains*

Xian-Sheng Liu(刘献省)[1], Yong-Guang Cheng(程永光)[2], Bao-He Yuan(袁保合)[3], Er-Jun Liang(梁二军)[4,†], and Wei-Feng Zhang(张伟风)[1,‡]

[1] *Henan Key Laboratory of Photovoltaic Materials and Low Dimensional Materials Science Laboratory, Henan University, Kaifeng* 475004, *China*
[2] *College of Science, Center of Analysis and Testing of Henan Institute of Engineering, Zhengzhou* 451191, *China*
[3] *North China University of Water Resources and Electric Power, Zhengzhou* 450011, *China*
[4] *School of Physical Science & Engineering and Key Laboratory of Materials Physics of Ministry of Education of China, Zhengzhou University, Zhengzhou* 450052, *China*

(Received 8 June 2019; revised manuscript received 10 July 2019; published online 7 August 2019)

Ceramics usually have irregular grains, cracking, or porosity, which result in their lightproof. $Y_2Mo_3O_{12}$ ceramics have more porosity due to the heavy hygroscopicity. Introducing ZnLi to $Y_2Mo_3O_{12}$ could form regular grains, reduce cracking and porosity. With increasing the content of ZnLi, the grain shapes self-assembly gradually and then the laser scattering and transmittance improve. The laser scattering property and transmittance of diverging rays become the best in ceramics $Y_{2-x}(ZnLi)_xMo_3O_{12}$ ($x = 1.0$ and 1.2) with regular grains and low thermal expansion. The formation mechanism of regular grains is ascribed to the substitutions of $Zn^{2+}$ and $Li^+$ for $Y^{3+}$ in $Y_2Mo_3O_{12}$ resulting in the preferential growth. The investigation in laser scattering, transmittance and low thermal expansion behaviors of $Y_{2-x}(ZnLi)_xMo_3O_{12}$ could pave a way to weaken the strong-laser attack from the high-power laser weapon and the other.

**Keywords:** low thermal expansion, laser scattering, regular grains, diverging rays transmittance

**PACS:** 65.40.De, 78.20.Ek, 81.05.Je, 81.10.Jt **DOI:** 10.1088/1674-1056/ab3435

## 1. Introduction

The harm on the aircrafts from a strong laser weapon is mortal although the strong laser undergoes the atmosphere refraction, absorption, scattering, turbulence, thermal blooming, and breakdown.[1–3] Scattering the laser beam to diverging rays with high transmittance rate by a protective layer on aircrafts is the optimal method to weaken the mortal attack from the high-power laser weapon. However, the protective layer could fall off due to thermal expansion on heating from laser. Negative thermal expansion (NTE) materials could find applications due to their abnormal thermal expansion properties and potential applications in realizing near-zero thermal expansion.[4–7] NTE mechanisms such as phonon anharmonicity, phase transition, charge transfer, Jahn–Teller effect, and nanoscale effect have been proposed to explain the NTE origin successfully for open framework structure materials, magnetic and ferroelectric materials, high pressure-phase $LaCu_3Fe_4O_{12}$ and $BiNiO_3$, etc.[4–18] Of the NTE materials, the $A_2M_3O_{12}$ ($A$: trivalent ion, $M$: W or Mo) family with larger NTE coefficients and stable open framework structure is very attractive, however the heavy hygroscopicity resulting in the disappearance of NTE near room temperature and the single function are the main obstacle for its applications to reduce the thermal expansion coefficient.[19–28] During the release process of crystal water, $A_2Mo_3O_{12}$ even shows an abrupt positive thermal expansion, and only after the complete release of crystal water, the NTE presents. To reduce the hygroscopicity of $A_2Mo_3O_{12}$, some trivalent ions have been employed separately to substitute the $A^{3+}$ ions, such as $Al^{3+}$, $Fe^{3+}$, $Cr^{3+}$, $La^{3+}$, $Ce^{3+}$: $Yb_{2-x}Al_xMo_3O_{12}$, $Fe_{2-x}Y_xMo_3O_{12}$, $Ln_{2-x}Cr_xMo_3O_{12}$ ($Ln$: Er, Y), $Y_{2-x}La_xMo_3O_{12}$, $Ce^{3+}/Y_2Mo_3O_{12}$.[20–24] Partial uni-ion substitution for $A^{3+}$ changes the large openings in the network[21] and the bond angle of $A$–O–M, therefore, the hygroscopicity of $A_2M_3O_{12}$ is reduced greatly. The primary orthorhombic structure of $Y_2Mo_3O_{12}$ changes in space group ($Pba2$ to $Pbcn$[29]), and even transforms to monoclinic[20,21,28] or tetragonal structures.

The above investigations suggest that it may be difficult to retain the orthorhombic structure after eliminating the hygroscopicity of $Y_2Mo_3O_{12}$ by the partial uni-ion substitution for $Y^{3+}$. The reason is ascribed to the different structures of monoclinic ($A^{3+}$ with smaller radius) or tetragonal ($A^{3+}$ with much larger radius) with orthorhombic ($A$–Y, Yb). Considering the orthorhombic structure of $Li_2Mg_2Mo_3O_{12}$,[30] in our recent investigation, two ions of $Li^+$ and $Mg^{2+}$ have been adopted as the substitution ions for $Y^{3+}$ and then the hygroscopicity

*Project supported by the National Natural Science Foundation of China (Grant Nos. 60976016, 61350012, and 11574276), the Key Scientific Research Projects of Henan Province, China (Grant No. 15B140004), Henan Science and Technology Development Project, China (Grant No. 182102210241), Key Projects of Science and Technology Research of Henan Provincial Department of Education, China (Grant No. 18A140014), and Industrial Science and Technology Research Projects of Kaifeng, Henan Province, China (Grant No. 1501049).

†Corresponding author. E-mail: ejliang@zzu.edu.cn
‡Corresponding author. E-mail: wfzhang@henu.edu.cn

© 2019 Chinese Physical Society and IOP Publishing Ltd 

of $Y_2Mo_3O_{12}$ was reduced.[31] However, detailed investigation suggested that even though remaining the orthorhombic structure, the x-ray diffraction (XRD) peaks changed so much that some orientations such as (102) and (131) were separate from the others due to the large radius difference between $Li^+$ (76 pm) and $Mg^{2+}$ (72 pm), consequently, the grain clearance was observed obviously. The result indicates that two ions with less radius difference should be under consideration to change the crystal structure moderately, so that the hygroscopicity and grain clearance are reduced together and multifunction could be realized.

In the present paper, considering the orthorhombic structure of $Li_2Zn_2Mo_3O_{12}$,[32,33] $Li^+$ (76 pm) and $Zn^{2+}$ (74 pm) with less radius difference as substitutions for $Y^{3+}$ are adopted to reduce the hygroscopicity and obtain regular grains. The orthorhombic structure changes gradually and the hygroscopicity decreases with increasing the content of $(LiZn)^{3+}$. The low thermal expansion ceramics $Y_{2-x}(ZnLi)_xMo_3O_{12}$ ($x = 1.0$ and 1.2) with regular grains possess excellent laser scattering property and high transmittance rate of diverging rays. The relationship between the laser scattering property/transmittance and regular grain is discussed.

## 2. Experiment

Analytical regents of $Y_2O_3$, $MoO_3$, ZnO, and $LiNO_3$ as raw materials were weighted according to the stoichiometric ratios of destination materials of $Y_{2-x}(ZnLi)_xMo_3O_{12}$ ($x = 0$, 0.1, 0.3, 0.5, 0.7, 0.9, 1.0, 1.2, 1.4, 1.6, 1.8, 2.0). The raw materials were mixed and ground for about 2 h. The mixtures were coldly pressed into pellets at pressure about 200 MPa followed by sintering at 1073 K for 5 h in air and then cooling down to room temperature naturally.

XRD measurements were carried out with a Bruker D8 Advance x-ray diffractometer to analyze the crystal structure. Raman spectra were recorded with a Renishaw inVia Raman spectrometer with 633 nm laser excitation. The microstructures and energy dispersive spectra of the samples were examined with a scanning electron microscopy (SEM, Model Quanta 250). The thermogravimetry (TG) and differential scanning calorimeter (DSC) measurements were carried out on a Netzsch STA 449F3 simultaneous thermal analyzer in the temperature range of 300–700 K, with the heating rates of 10 K/min. The linear coefficients of thermal expansion (CTE) were measured with a dilatometer (Linseis DIL L76). The laser with wavelength of 633 nm and power of about 50 mW passed through a microscope objective lens connecting with the Raman spectrometer. The laser is a He–Ne laser with the brand of Renishaw. The red laser (633 nm) scattering pictures were recorded with a digital camera (Canon 100D).

## 3. Results and discussion

### 3.1. Laser scattering property and regular grains formation of $Y_{2-x}(ZnLi)_xMo_3O_{12}$

Figures 1(a)–1(e) show the red laser (633 nm) scattering pictures of $Y_{2-x}(LiZn)_xMo_3O_{12}$ with $x = 0.3$, 0.7, 1.0, 1.2, and 1.8. For the ceramic sample with $x = 0.3$ (Fig. 1(a)), when a laser beam (633 nm) illuminates the surface of the ceramic block, the laser beam is scattered and half of the ceramic block becomes bright because some diverging rays are transmitted. The bright field is larger than half of the ceramic block for the ceramic sample with $x = 0.7$ (Fig. 1(b)). Especially, for the ceramic samples with $x = 1.0$ and 1.2, the whole ceramic blocks are bright and much more diverging rays are transmitted (Figs. 1(c) and 1(d)). However, only much size is bright for the ceramic sample with $x = 1.8$ (Fig. 1(e)).

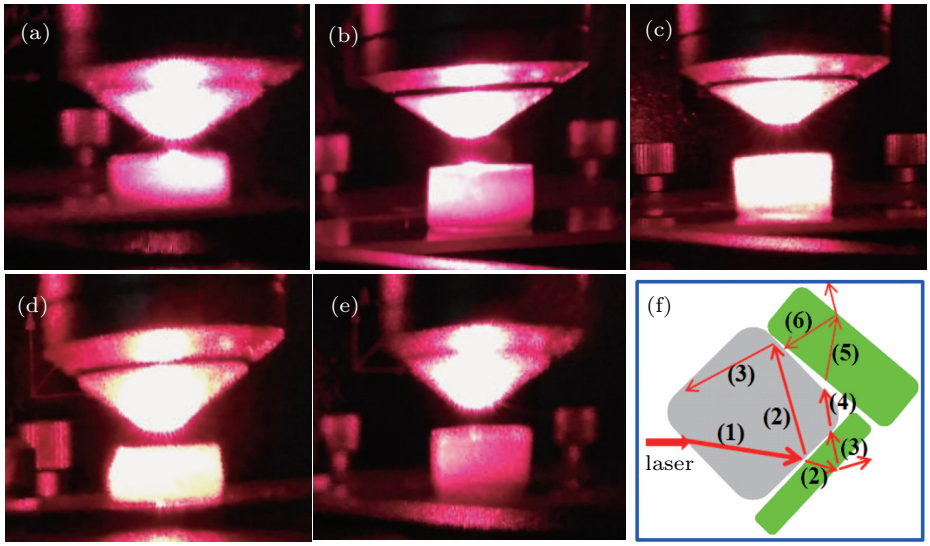



**Fig. 1.** (a)–(e) Red laser scattering and transmittance pictures of $Y_{2-x}(LiZn)_xMo_3O_{12}$ with $x = 0.3$, 0.7, 1.0, 1.2, and 1.8. The laser beam is focused on the upper surface center of the pellets. The diameters of the pellets are about 0.8 cm. The heights of the pellets are about (a) 5 mm, (b) 5 mm, (c) 6 mm, (d) 5 mm, and (e) 6 mm. (f) Schematic diagram of laser scattering and transmittance in the ceramic grains.

The laser scattering is reported to relate to the size of the ceramic particles.[34] In general, when a laser beam illuminates the surface of a ceramic, the laser beam will be absorbed and scattered partly. Laser scattering could be divided into three types: Rayleigh ($a_0 \ll \lambda$), Mie ($a_0 \sim \lambda$), and Tyndall ($a_0 \gg \lambda$), where $a_0$ is the size of the scattering center and $\lambda$ is the laser wavelength. For Rayleigh ($a_0 \ll \lambda$) and Mie ($a_0 \sim \lambda$) scatterings, the scattering cross section relates to $\delta = \lambda/2r$. The scattering coefficient increases with the size of the scattering microspheres when the sphere diameter is smaller than the wavelength and reaches the maximum when the particle size equals to the laser wavelength, and thereafter decreases with the particle size.

In order to explore the effects of the grain size and pores on the laser scattering phenomenon, the microstructure of $Y_{2-x}(LiZn)_xMo_3O_{12}$ was investigated with SEM. Figure 2 shows the SEM images of $Y_{2-x}(LiZn)_xMo_3O_{12}$ with different contents of $(LiZn)^{3+}$. For pure $Y_2Mo_3O_{12}$ (Fig. 2(a)), squeezed together spherical grains are separated with each others by some pores due to the influence of crystal water and air left in the ceramics. For $x = 0.3$ (Fig. 2(b)), even though with less content of $(LiZn)^{3+}$ in $Y_2Mo_3O_{12}$, the air pores in the ceramics are reduced largely and much larger spherical grains appear. When the content reaches $x = 0.7$ (Fig. 2(c)), the regular quadrangular prisms and tetrahedral are observed, i.e., the grains appear edges and corners rather than mere circular arcs, however, air pores still exist. For $x = 1.0$ (Fig. 2(d)), larger regular grains contact with each other along straight edges and some smaller grains fill in the clearance among particles, therefore, there are much less pores. Then there appear some octahedra, rods among the grains with straight edges (see image of the sample with $x = 1.2$ in Fig. 2(e)), which grow along the slits among the larger grains.

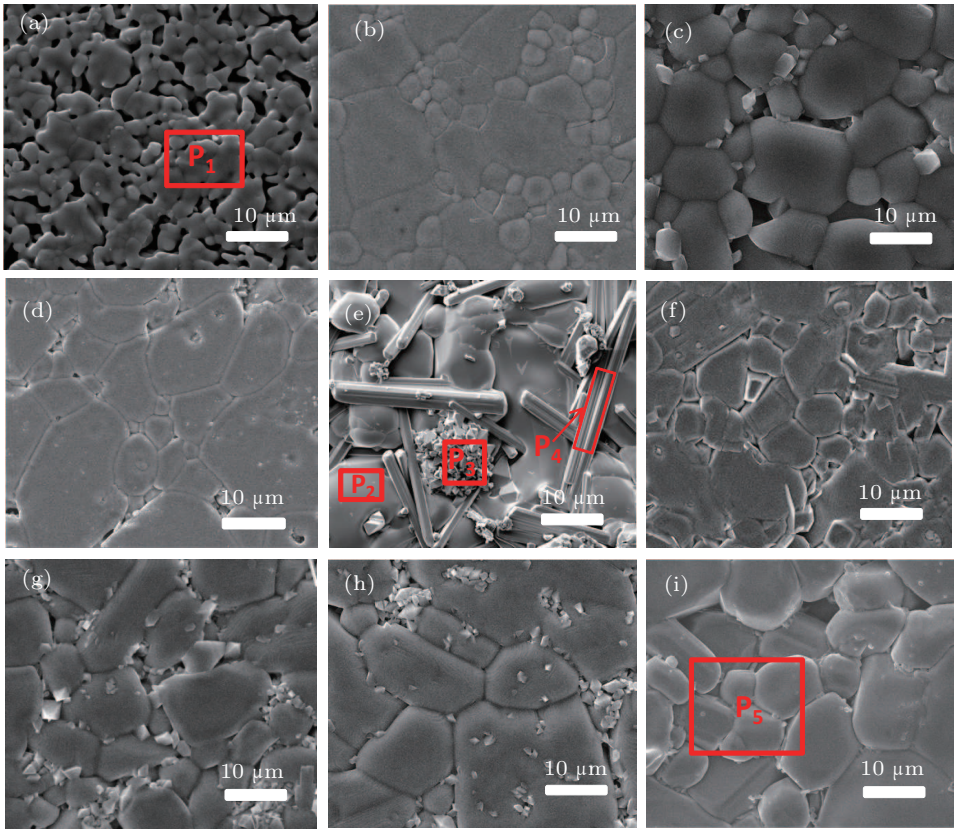



**Fig. 2.** (a)–(h) SEM images of $Y_{2-x}(LiZn)_xMo_3O_{12}$ with $x = 0$, 0.3, 0.7, 1.0, 1.2, 1.4, 1.6, 1.8, and 2.0. The grain shapes change remarkably with increasing the content of $(LiZn)^{3+}$.

The continuous change in grain shapes rather than the grain sizes is found with increasing the content of $(LiZn)^{3+}$ in $Y_2Mo_3O_{12}$. The results suggest that the grain shapes in $Y_{2-x}(LiZn)_xMo_3O_{12}$ ceramics could change the laser scattering behavior. The transmittance of diverging rays could also be related to the regular grains and density of the ceramics. The regular grains have less porosity and high density.

The octahedra and rods have more content of $(LiZn)^{3+}$ in $Y_2Mo_3O_{12}$ and the larger grains with straight edges have lower content of $(LiZn)^{3+}$, which can be discerned from the relative intensities of the peaks of Zn, Y, Mo in the EDS spectra (see Figs. 3(a)–3(e)). For $x = 1.4$ (Fig. 2(f)), the amount of $(LiZn)^{3+}$ takes up the majority in $Y_{2-x}(LiZn)_xMo_3O_{12}$, i.e., $Y^{3+}$ as a substitution ion, the tetrahedra are of $(LiZn)_2Mo_3O_{12}$ with certain amount of $Y^{3+}$. The grains grow along the substitution direction to form the rods/point ends according to the

lowest energy principle along the substitution direction. However, excess $(LiZn)^{3+}$ induces some pores even though some small grains fill in the pores (Figs. 2(g) and 2(h)). Therefore, a suitable amount of (LiZn) is critic for high relative density of $Y_{2-x}(LiZn)_xMo_3O_{12}$, which results from the filling effect of the small grains. Though the theory densities increase with increasing the substitution of $(LiZn)^{3+}$ for $Y^{3+}$ in $Y_2Mo_3O_{12}$, the relative density of ceramics $Y_{2-x}(LiZn)_xMo_3O_{12}$ increases with increasing $x$ to the maximum of 92.85% ($x = 1.0$) and then decreases (Fig. 3(f)).

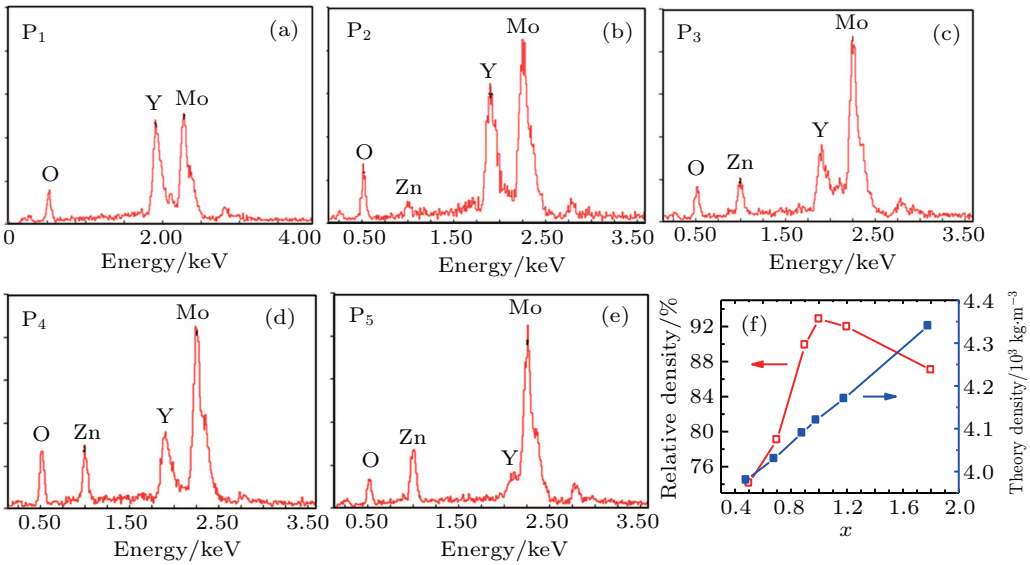



**Fig. 3.** EDS spectra of $Y_{2-x}(LiZn)_xMo_3O_{12}$ with (a) $x = 0$, (b)–(d) 1.2, and (e) 2.0. (f) Theory density and relative density curves of $Y_{2-x}(LiZn)_xMo_3O_{12}$ with $x = 0.5$, 0.7, 0.9, 1.0, 1.2, and 1.8.

The remarkable change in the microstructure of $Y_{2-x}(LiZn)_xMo_3O_{12}$ is analyzed from sintering behavior as follow. The raw materials of $Y_2O_3$ and $MoO_3$ are compacted in a cylindrical mold via point contact containing air pores under pressure. During the sintering process, atoms (Y, Mo, O) and molecules ($Y_2O_3$ and $MoO_3$) rapid scatter and then a chemical conversion ($Y_2O_3+3MoO_3 \rightarrow Y_2Mo_3O_{12}$) takes place, changing the shape and position of the particles and internal pores. Consequently, smaller particles with larger total surface area transform to lager particles with less total surface area, which are energetically more favorable than the smaller ones. During the cooling process, $Y_2Mo_3O_{12}$ expands and some crystal water invades into the crystal from the microchannels. With introducing ZnO and $LiNO_3$ in the raw materials, $Zn^{2+}$ and $Li^+$ enter into the lattice and substitute $Y^{3+}$ in $Y_2Mo_3O_{12}$, resulting in the shrinkage of microchannels and thereafter reduction of crystal water and air pores. The destructive effect of crystal water on crystal structure could be weakened and the high-temperature crystal structure remains to room temperature. A reduction of grain-boundary-surface energy ratio could be obtained and consequently the densification increases.[35] On the other hand, the crystal grows rapidly along the direction of substitution of $(LiZn)^{3+}$ for $Y^{3+}$ due to the lowest energy principle and cylinder/rod particles appear.

Therefore, for the present case, the regular grains and less porosity together should be responsible for the laser scattering and transmittance of diverging rays. Figure 1(f) shows the schematic diagram of laser beam brightening the ceramic grains. A laser beam is scattered by the regular ceramic grains and weak rays exit from the ceramic surface, therefore, the laser energy is dispersed by the ceramic grains. The scattering property of the ceramics could effectively reduce the killing effect of strong laser, whose high energy focus on the surface might melt the target. If the military aircrafts are coated with the as-prepared ceramic $Y_{2-x}(LiZn)_xMo_3O_{12}$ with $x = 1.0$ and 1.2, the high energy of the strong laser from laser guns could be dispersed to diverging rays by the coating layer and the military aircrafts might be safe.

### 3.2. Crystal structure

Figure 4(a) shows XRD patterns of $Y_{2-x}(LiZn)_xMo_3O_{12}$ with $x$ from 0 to 2.0 at room temperature (the left part presents the diffraction of $2\theta$ from 15° to 40°, while the right part corresponds to $2\theta$ from 25° to 27°). For $x = 0$, there are only a few broad diffraction peaks due to heavy hygroscopicity,[19] which indicates that the crystal water in the lattice lowers the crystal quality of $Y_2Mo_3O_{12}$ to form amorphous structure. Crystal water molecules in the lattice drag $Y^{3+}$ and nearest oxygen ion[24] distorting the growth along crystal plains, which results in less difference between the crystal plains and broadened diffraction peaks.

With increasing the content of $(LiZn)^{3+}$ from $x = 0.1$ to $x = 0.9$, the diffraction peaks become sharp, some new peaks corresponding to *Pba*2-$Y_2Mo_3O_{12}$ appear, and some peaks

split. For example, the broad diffraction peak about 25.5° according to *Pba*2-$Y_2Mo_3O_{12}$ splits into two peaks at 25.4° and 25.6° (right in Fig. 4(a)), indicating the quality enhancement of the crystal plains of $Y_2Mo_3O_{12}$. It is believed that, with increasing the content of $(LiZn)^{3+}$, smaller ions of $Li^+$ (76 pm) and $Zn^{2+}$ (74 pm) partially substitute the larger ion of $Y^{3+}$ (90 pm) to shrink the microchannels in the lattice of $Y_2Mo_3O_{12}$ and induce the growth orientation of $Y_2Mo_3O_{12}$ crystal (the relative intensities of diffraction peaks are different from those of *Pba*2-$Y_2Mo_3O_{12}$ at 423 K[29]), which results in the decrease of crystal water. However, the transformation from space group *Pba*2 to *Pbcn*[29] during the temperature increasing process is not observed, which suggests the different effects between temperature and ion-substitution on the decrease of crystal water. With increasing temperature, the average kinetic energies of crystal water molecules increase enough and run away from the lattice of $Y_2Mo_3O_{12}$. The relative sites of $Y^{3+}$, $Mo^{6+}$, and $O^{2-}$ change obviously, which results in the change of symmetry. However, with increasing the content of $(LiZn)^{3+}$ to substitute $Y^{3+}$, crystal water molecules are repelled out of the lattice. The lattice changes a little due to the substitution of $(LiZn)^{3+}$. When the content of $(LiZn)^{3+}$ reaches $x = 1.0$, the lattice changes enough and there appear some new peaks such as peaks at about 25.9° and 26.3°, which are corresponding to $(LiZn)_2Mo_3O_{12}$. From $x = 1.0$ to $x = 1.4$, there are two phases of *Pba*2-$Y_2Mo_3O_{12}$ and $(LiZn)_2Mo_3O_{12}$. From $x = 1.6$ to $x = 2.0$, there is only a single phase of $(LiZn)_2Mo_3O_{12}$.

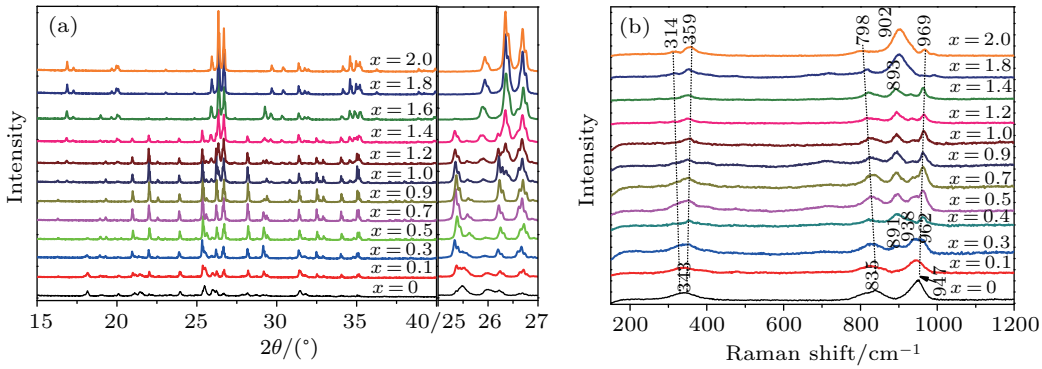



**Fig. 4.** (a) XRD patterns and (b) Raman spectra of $Y_{2-x}(LiZn)_xMo_3O_{12}$ with $x$ from 0 to 2.0 at room temperature.

Figure 4(b) shows Raman spectra of $Y_{2-x}(LiZn)_xMo_3O_{12}$ with $x$ from 0 to 2.0 at room temperature. For pure $Y_2Mo_3O_{12}$, there are only broad peaks at about 343 $cm^{-1}$, 835 $cm^{-1}$, and 947 $cm^{-1}$ due to the effect of crystal water on the vibrations, which are assigned to symmetric and asymmetric bending motions in both $YO_6$ octahedra and $MoO_4$ tetrahedra, symmetric and asymmetric stretching vibrations of the $MoO_4$ tetrahedra.[15,19,21] With increasing the content of $(LiZn)^{3+}$, the vibrations of Y–O and Mo–O are affected so strongly that the Raman peaks become sharp and the peaks split: the peak at 343 $cm^{-1}$ splits into 314 $cm^{-1}$ and 359 $cm^{-1}$ and the peak at 947 $cm^{-1}$ splits into 895 $cm^{-1}$, 938 $cm^{-1}$, and 951 $cm^{-1}$. Even though the peak splitting appears, there is no characteristic peak showing the monoclinic structure.[20,21] The result indicates that the crystal phase is still orthorhombic.

### 3.3. Hygroscopicity reduction and low thermal expansion property

In order to show the hygroscopicity reduction of $Y_2Mo_3O_{12}$ with increasing content of $(LiZn)^{3+}$, the TG measurements of $Y_{2-x}(LiZn)_xMo_3O_{12}$ were performed (see Fig. 5(a)). The amount of crystal water in the samples with different contents of $(LiZn)^{3+}$ can be estimated with TG curves: $Y_2Mo_3O_{12}{\cdot}2.97$ $H_2O$, $Y_{1.9}(LiZn)_{0.1}Mo_3O_{12}{\cdot}0.84$ $H_2O$, $Y_{1.5}(LiZn)_{0.5}Mo_3O_{12}{\cdot}0.38$ $H_2O$, $Y_{1.1}(LiZn)_{0.9}Mo_3O_{12}{\cdot}0.18$ $H_2O$. The results confirm that the substitutions of $(LiZn)^{3+}$ decrease the hygroscopicity obviously. The samples ($x = 1.0$ and 1.2) with highest transmission rate of diverging rays have no hygroscopicity. This suggests that the laser scattering and transmittance of diverging rays could also be influenced by crystal water, which is consisted with the result from Fig. 1.

The relative length changes of $Y_{2-x}(LiZn)_xMo_3O_{12}$ with different contents of $(LiZn)^{3+}$ were measured with increasing temperature (Fig. 5(b)). For $x = 0.0$ (pure $Y_2Mo_3O_{12}$), there are two expansion processes and two contraction processes corresponding to the release of adsorbed water and crystal water. Only after the complete release of crystal water, the NET phenomenon is observed. With increasing the content of $(LiZn)^{3+}$, the thermal expansion and contraction parts corresponding to the release of crystal water become weakened, indicating that the heavy hygroscopicity is reduced remarkably. For the sample of $x = 0.7$, much lower thermal expansion (CTE $\alpha = 5.79 \times 10^{-6}$ $K^{-1}$, 480–670 K) than that of $x = 2.0$ (CTE $\alpha = 19.21 \times 10^{-6}$ $K^{-1}$, 290–670 K) is obtained besides the reduced hygroscopicity. For the samples of $x = 1.0$ and 1.2, the hygroscopicity is deleted completely and the CTEs ($\alpha_{1.0} = 13.66 \times 10^{-6}$ $K^{-1}$, $\alpha_{1.2} = 16.24 \times 10^{-6}$ $K^{-1}$, 290–670 K) are reduced obviously comparing with that of $x = 2.0$.

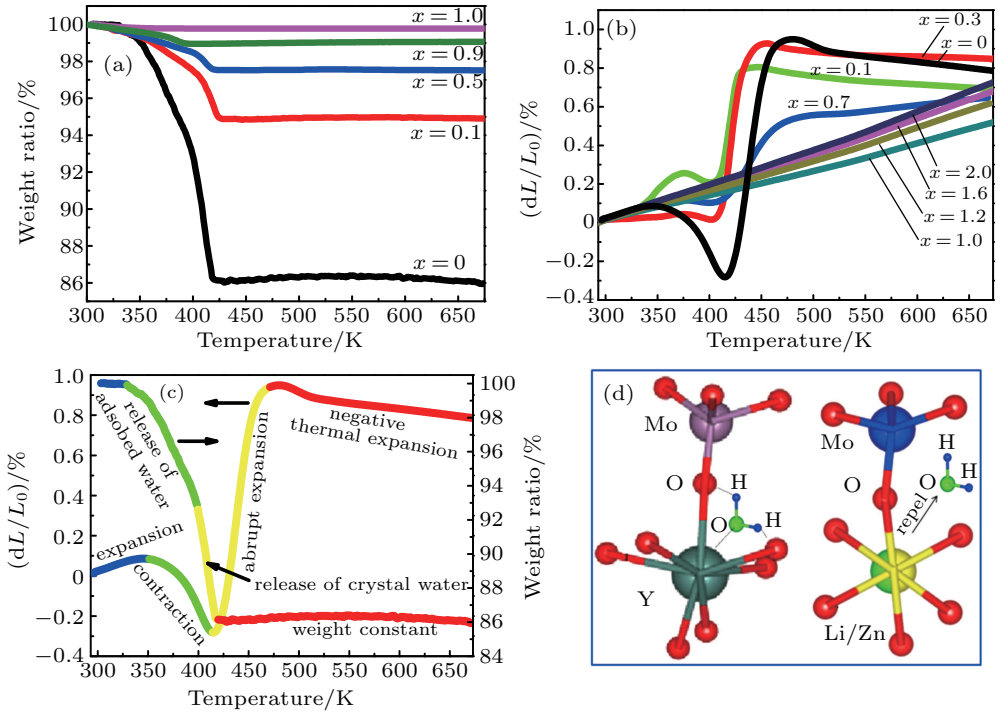



**Fig. 5.** (a) The TG curves and (b) relative length changes of $Y_{2-x}(LiZn)_xMo_3O_{12}$ with different contents of (LiZn). (c) Different effects of absorbed water and crystal water release on the thermal expansion property of $Y_2Mo_3O_{12}$: left axis presents the relative length change of $Y_2Mo_3O_{12}$; right axis presents the TG of $Y_2Mo_3O_{12}$. (d) Schematic diagram of the effect of (LiZn) substitutions on crystal water.

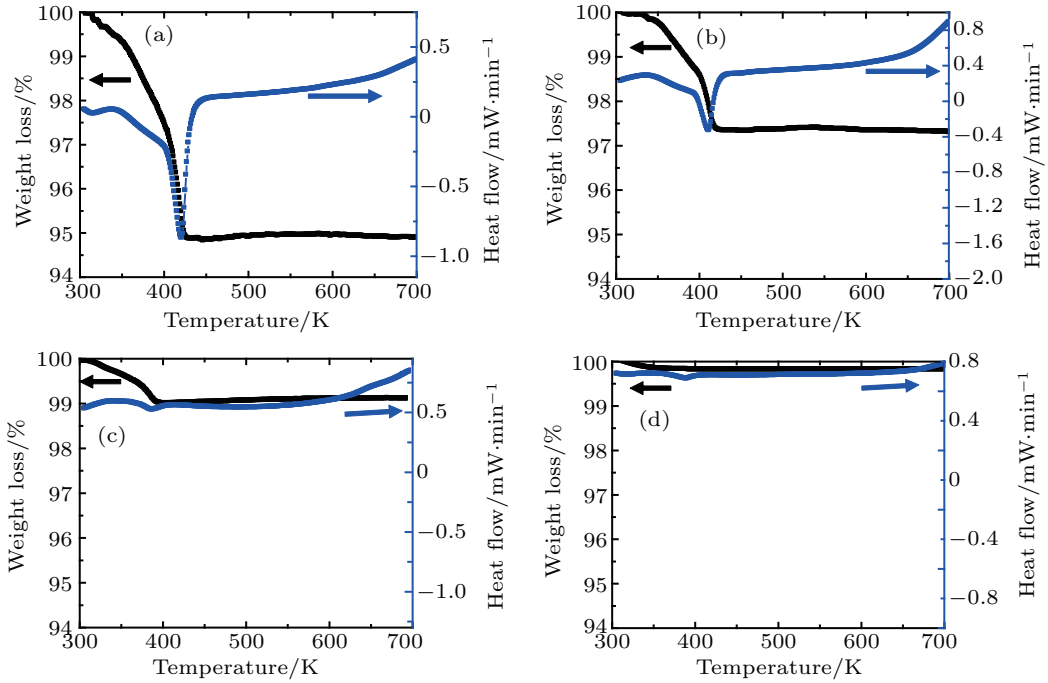



**Fig. 6.** TG-DSC curves of $Y_{2-x}(LiZn)_xMo_3O_{12}$ with different contents ((a)–(d) $x = 0.1, 0.5, 0.9, 1.0$) of (LiZn).

Figures 5(a) and 5(b) show that the release process of crystal water is usually accompanied by the relative length change. Therefore, the two expansion processes and two contraction processes of pure $Y_2Mo_3O_{12}$ ($x = 0.0$) are drawn together with the release processes of water. Before the release of adsorbed water (blue line part in Fig. 5(c)), the crystal lattice expands with increasing temperature. During the release process of adsorbed water (green line part in Fig. 5(c)), the lattice contracts just like the contraction of seeds by releasing the adsorbed water. For the release process of crystal water (yellow line part in Fig. 5(c)), the lattice presents abrupt expansion and hysteresis. Only after the complete release of crystal water (red line part in Fig. 5(c)), the NET phenomenon is observed. The reduction of hygroscopicity is discussed as follows: the substitutions of $Li^+$ and $Zn^{2+}$ for $Y^{3+}$ cause one and two electrons less than the needed three electrons, and then two type

ions of $(Li_Y)^{2-}$ and $(Zn_Y)^{-}$ form to repel the oxygen in $H_2O$ (Fig. 5(d)).

In order to investigate the water change with temperature of $Y_{2-x}(LiZn)_xMo_3O_{12}$ with different contents ($x = 0.1$, 0.5, 0.9, 1.0) of (LiZn), TG-DSC curves are presented (Figs. 6(a)–6(d)), where the axis of weight loss is from 100% to 94% for comparison. For $x = 0.1$, the release process of adsorbed water reaches $\sim 97\%$, much less than $\sim 93\%$ of $x = 0.0$ (Fig. 5(c)). The release process of crystal water is from $\sim 97\%$ to 95%, also less than that from $\sim 93\%$ to 86% of $x = 0.0$ (Fig. 5(c)). It shows that the adsorbed water and crystal water of the sample with $x = 0.1$ are less than those of the sample with $x = 0.0$. With increasing $x$ from 0.5 to 1.0, the adsorbed water and crystal water reduce remarkably, even close to zero for $x = 1.0$.

## 4. Conclusion

The relationships of the laser scattering/transmittance of diverging rays, regular grains, and porosity of $Y_{2-x}(LiZn)_xMo_3O_{12}$ with $x$ from 0 to 2.0 are investigated. It is found that the as-prepared ceramic $Y_{2-x}(LiZn)_xMo_3O_{12}$ with $x = 1.0$ and 1.2 present excellent laser scattering/transmittance, regular grains, and less porosity, no hygroscopicity. The result suggests that a certain amount of $(LiZn)^{3+}$ leads to the reduction of hygroscopicity, the formation of regular grains, less porosity, and then excellent laser scattering/transmittance of diverging rays. The low thermal expansion ceramics of $Y_{2-x}(LiZn)_xMo_3O_{12}$ with $x = 1.0$ and 1.2 could find applications in coating layer with properties of laser scattering and transmittance of diverging rays for reducing harm from strong laser beam.

## References


[1] Song L, Ma H, Cheng Y J and Zou Y J 2014 *Ship Electron. Eng.* **34** 162
[2] Wang X B and Ma Z Z 2012 *Equip. Environ. Eng.* **9** 33
[3] Wohlers M R 1972 *Appl. Opt.* **11** 1389
[4] Takenaka K, Okamoto Y, Shinoda T, Katayama N and Sakai Y 2017 *Nat. Commun.* **8** 14102
[5] Monroe J A, Gehring D, Karaman I, Arroyave R, Brown D W and Clausen B 2016 *Acta Mater.* **102** 333
[6] Ahadi A, Matsushita Y, Sawaguchi T, Sun Q P and Tsuchiya K 2017 *Acta Mater.* **124** 79
[7] Chen J, Wang F F, Huang Q Z, Hu L, Song X P, Deng J X, Yu R B and Xing X R 2013 *Sci. Rep.* **3** 2458
[8] Yan J, Sun Y, Wang C, Chu L H, Shi Z X, Deng S H, Shi K W and Lu H Q 2014 *Scr. Mater.* **84-85** 19
[9] Hu L, Chen J, Fan L L, Ren Y, Rong Y C, Pan Z, Deng J X, Yu R B and Xing X R 2014 *J. Am. Chem. Soc.* **136** 13566
[10] Chen J, Gao Q L, Sanson A, Jiang X X, Huang Q Z, Carnera A, Rodriguez C G, Olivi L, Wang L, Hu L, Lin K, Ren Y, Lin Z S, Wang C, Gu L, Deng J X, Attfield J P and Xing X R 2017 *Nat. Commun.* **8** 14441
[11] Lama P, Das R K, Smith V J and Barbour L J 2014 *Chem. Commun.* **50** 6464
[12] Bridges F, Keiber T, Juhas P, Billinge S J L, Sutton L, Wilde J and Kowach G R 2014 *Phys. Rev. Lett.* **112** 045505
[13] Pryde A K A, Hammonds K D, Dove M T, Heine V, Gale J D and Warren M C 1996 *J. Phys.: Condens. Matter.* **8** 10973
[14] Zhang M D, Mao Y C, Guo J, Zhou W J, Chao M J, Zhang N, Yang M J, Kong X H, Kong X S and Liang E J 2017 *RSC Adv.* **7** 3934
[15] Wang L, Wang F, Yuan P F, Sun Q, Liang E J, Jia Y and Guo Z X 2013 *Mater. Res. Bull.* **48** 2724
[16] Goodwin A L, Calleja M, Conterio M J, Dove M T, Evans J S O, Keen D A, Peters L and Tucker M G 2008 *Science* **319** 794
[17] Long Y W, Hayashi N, Saito T, Azuma M, Muranaka S and Shimakawa Y 2009 *Nature* **458** 60
[18] Azuma M, Chen W T, Seki H, Czapski M, Olga S, Oka K, Mizumaki M, Watanuki T, Ishimatsu N, Kawamura N, Ishiwata S, Tucker M G, Shimakawa Y and Attfield J P 2011 *Nat. Commun.* **2** 347
[19] Liang E J, Huo H L, Wang J P and Chao M J 2008 *J. Phys. Chem. C* **112** 6577
[20] Li Q J, Yuan B H, Song W B and Liang E J 2012 *Chin. Phys. B* **21** 046501
[21] Li Z Y, Song W B and Liang E J 2011 *J. Phys. Chem. C* **115** 17806
[22] Wu M M, Hu Z B, Liu Y T and Chen D F 2009 *Mater. Res. Bull.* **44** 1943
[23] Liu H F, Wang X C, Zhang Z P and Chen X B 012 *Ceram. Int.* **L38** 6349
[24] Liu X S, Cheng Y G, Liang E J and Chao M J 2014 *Phys. Chem. Chem. Phys.* **16** 12848
[25] Liu X S, Ge X H, Liang E J and Zhang W F 2017 *Chin. Phys. B* **26** 108101
[26] Liu X S, Yuan B H, Cheng Y G, Ge X H, Liang E J and Zhang W F 2017 *Phys. Chem. Chem. Phys.* **19** 13443
[27] Yang G, Sun X W, Liang E J and Zhang W F 2018 *Ceram. Int.* **44** 22032
[28] Liu X S, Cheng Y G, Yuan B H, Liang E J and Zhang W F 2019 *J. Alloys Compd.* **776** 236
[29] Gates S D and Lind C 2007 *J. Solid State Chem.* **180** 3510
[30] Trifonov V A, Pavlyuk A A, Gorbachenya K N, Yasyukevich A S and Kuleshov N V 2013 *Inorg. Mater.* **49** 517
[31] Cheng Y G, Liu X S, Song W B, Yuan B H, Wang X L, Chao M J and Liang E J 2015 *Mater. Res. Bull.* **65** 273
[32] Xue L P, Wang Y J, Lv P W, Chen D G, Lin Z, Liang J K, Huang F and Xie Z 2009 *Cryst. Growth* . **9** 914
[33] Yang X L, Zheng Y, Liu Z L and Dong Z W 2016 *Electron. Compo. Mater.* **35** 6
[34] He G S, Qin H Y and Zheng Q 2009 *J. Appl. Phys.* **105** 023110
[35] Prochazka S and Scanlan R M 1975 *J. Am. Ceram. Soc.* **58** 72